Interaction of elastocapillary flows in parallel microchannels across a thin membrane

S. P. Reddy, R. A. Samy, and A. K. Sen

Citation: Appl. Phys. Lett. **109**, 141601 (2016); doi: 10.1063/1.4964264
View online: http://dx.doi.org/10.1063/1.4964264
View Table of Contents: http://aip.scitation.org/toc/apl/109/14
Published by the American Institute of Physics

Interaction of elastocapillary flows in parallel microchannels across a thin membrane

S. P. Reddy, R. A. Samy, and A. K. Sen[a)]
Department of Mechanical Engineering, Indian Institute of Technology Madras, Chennai 600036, India

(Received 20 August 2016; accepted 22 September 2016; published online 3 October 2016)

We report the interaction of counter elastocapillary flows in parallel microchannels across a thin membrane. At the crossing point, the interaction between the capillary flows via the thin membrane leads to significant retardation of capillary flow. The drop in velocity at the crossing point and velocity variation after the crossing point are predicted using the analytical model and measured from experiments. A non-dimensional parameter J, which is the ratio of the capillary force to the mechanical restoring force, governs the drop in velocity at the crossing point with the maximum drop of about 60% for $J = 1$. The meniscus velocity after the crossing point decreases ($J < 0.5$), remains constant ($0.5 < J < 0.6$), or increases ($J > 0.6$) depending on the value of J. The proposed technique can be applied for the manipulation of capillary flows in microchannels. *Published by AIP Publishing.*
[http://dx.doi.org/10.1063/1.4964264]

Transport of liquids in microfluidic devices is enabled by various passive and active techniques.[1] Even though active techniques hold better control and higher throughput, passive techniques such as capillary flows are the most sought-after techniques owing to their simplicity, lean design, ease of operation, and power-free nature.[2] The interest towards passive techniques has resulted in an unprecedented research progress in capillary flows in microchannels and, in turn, leads to many interesting studies including elastocapillarity[3–7] and paper microfluidics.[8,9] Dynamics of capillary flow in nanochannels has been studied recently.[10,11] In nanochannels, due to relatively higher Laplace pressure, liquid condensation and gas dissolution have a considerable effect on the capillary filling dynamics.[11] The lack of control in the case of capillary flows in micro and nano channels has been reported as the major limitation of the technique.[12] Enhanced flow velocity can lead to faster response whereas flow retardation can provide longer incubation time.[13,14] Enhancement of capillary flow in a flexible channel in comparison to that in an identical rigid channel was reported.[3,4] Passive transport of a liquid plug by increasing the radius of curvature at one of its ends with the help of elastocapillary flow was achieved.[5] Pre-programmed and self-powered microfluidic circuits have been built from capillary elements.[15] However, this can only be attained by carefully designing the channel, making the design highly specific. Apart from shape and size, passive flow control of liquid at a specified position can also be achieved through surface patterning[16] and material modification. A complex fabrication procedure and lack of versatility in the design are bound to this method. Another technique used to control capillary flow is by changing channel geometry due to membrane deflection caused by mechanical actuators.[17] Capillary flow of a primary liquid (PL) was retarded or stopped with the help of a control fluid by varying the pressure of the control fluid.[17] Although the driving mechanism is passive, an external actuator is required to control the flow in either of these techniques. Here, we report the control of capillary flow due to the interaction of counter capillary flows in parallel adjoining microchannels across a thin membrane. By using theoretical model and experiments, control of capillary flow of a primary liquid with the help of capillary flow of a controlling liquid (CL) is demonstrated. We showed that it is possible to achieve a significant drop in velocity at the crossing point and control velocity after the crossing point by appropriate selection of a nondimensional parameter J which governs elastocapillary flow.

The device was fabricated by bonding two straight PDMS (polydimethylsiloxane) microchannels with a thin PDMS membrane bonded between the two (Fig. 1(a)). The microchannels (width 700–1300 μm and height 75–120 μm) were prepared using photolithography followed by soft lithography using PDMS polymer (Sylgard 184, Dow Corning).[18] Thin membranes of thickness 25–50 μm were prepared by spin coating the prepolymer on a plexiglass sheet and baking in an oven. The membrane and channels were bonded together after oxygen-plasma exposure. The device was used at least 6–8 h after the bonding to allow time for the surface properties to stabilize. The device was mounted horizontally on the stage of an inverted microscope (AxioVert A1, Zeiss). Droplets of liquid (0.1 ml) were generated at the ends of two capillaries connected to a syringe pump via a T-connector (Fig. 1(b)). The ends of the capillaries were held vertically, one at each inlet, to insert droplets simultaneously into both inlets. Please note that the droplets are introduced into the channel at atmospheric pressure and zero initial velocity so there is no influence of the syringe pump on the capillary flow of liquid in the channels. Experiments were performed with different liquids: mineral oil, silicone oil, and propan-1, 2-diol. The position of the menisci in the primary channel (PC) and controlling channel (CC) was recorded with a high speed camera (FASTCAM SA3, Photron) attached to the microscope. The distance travelled by the liquid menisci with respect to time was obtained using the scales engraved alongside the channels.

[a)]Author to whom correspondence should be addressed. Electronic mail: ashis@iitm.ac.in

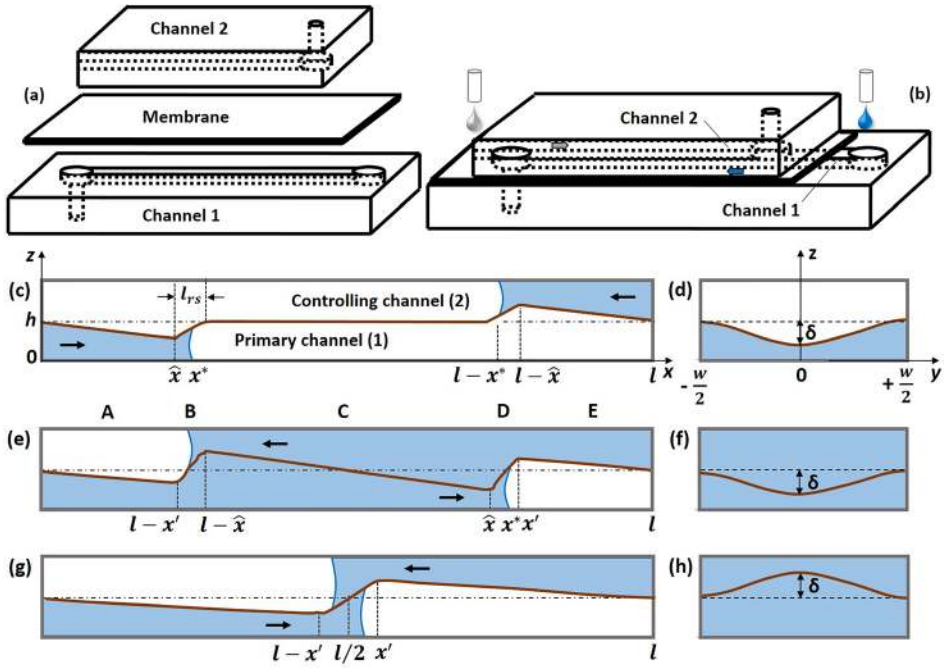

FIG. 1. (a) Exploded view of the PDMS microchannel device. (b) Insertion of liquids at the inlets of the PC and CC during experiments. Schematic diagram showing positions of PL and CL menisci and membrane deflection pattern (c) before the crossing point, x-z cross-sectional view, menisci of PL and CL are, respectively, at x^* and $l-x^*$, point of maximum inward deflection for PL and CL, respectively, at $\hat{x}$ and $l-\hat{x}$ (d) before the crossing point, y-z cross-sectional view, (e) after the crossing point, x-z cross-sectional view, point of maximum outward deflection at x' and $l-x'$ (f) after the crossing point, y-z cross-sectional view, (g) at the crossing point, x-z cross-sectional view, and (h) at the crossing point, y-z cross-sectional view.

For theoretical modeling, consider a thin rectangular membrane of flexural rigidity D, Poisson's ratio ν, width w, length l, and thickness t_m with its edges $y=\pm w/2$ built-in (Figs. 1(c)–1(h)). The membrane is sandwiched between two identical rectangular microchannels (i.e., primary and controlling channels, also referred to as channels 1 and 2, respectively) of width w and height h ($w \gg h$) and length l. We take that liquids in both channels are the same and moreover, they are inserted into the corresponding inlets at the same time so the menisci cross each other at $x=l/2$. Quasi-static analysis of the membrane is adequate since the characteristic time scale of capillary flow is much larger than the reaction time of the membrane to the load due to Young-Laplace pressure.[19] Since $Re \ll 1$, fluid inertia is negligible compared to viscous force and flow can be assumed to be quasi-static. Depending on the relative position of the menisci, we analyze the problem: before the crossing point, at the crossing point, and after the crossing point.

First, we consider a case before the liquids in the primary channel (PC) and controlling channel (CC) cross each other (Figs. 1(c) and 1(d)). Let us assume that the liquids are sufficiently far away from each other so that the controlling liquid (CL) has no influence on the primary liquid (PL). In that case, the dynamics of liquid in the PC is similar to that of a liquid present in a single flexible channel that we reported earlier.[4] Two deflection extrema each at $\hat{x}$ and $l-\hat{x}$ are present in the deformed membrane profile, each owing to the Young-Laplace pressure jump across the corresponding meniscus. The distance travelled by the meniscus x^* with time t in the PC is given by[4] modified Washburn's law as $x^*(t)=W_d\sqrt{t}$ and modified Washburns' constant W_d is given in Eq. (S1) (supplementary material). The effect of wall compliance appears in the non-dimensional parameter $J=4\alpha\left(\frac{h}{l_{ec}}\right)^2 a^4$ which is the ratio of surface tension force to elastic deformation force, $l_{ec}=\sqrt{D/\sigma\cos\theta}$ is the elastocapillary length. The value of constant $\alpha=1/386$ (from simulations[4]), a is the channel aspect ratio ($a=w/h$), σ is the surface tension of the liquid, and θ is the contact angle of the liquid with channel wall. From $x^*(t)=W_d\sqrt{t}$, velocity of the meniscus is obtained as $v_s=\frac{dx^*}{dt}=\frac{W_d^2}{2}\frac{1}{x^*}$, which is rearranged to seek the effect of J as, $\tilde{u}=\frac{1}{J}\left(\frac{\beta h}{3l}\right)\frac{F_1(\hat{\xi})}{\Gamma X}$, $\tilde{u}$ is the non-dimensional velocity given by v_s/U_{cap}, where U_{cap} is the capillary velocity given by[20] $\frac{\sigma\cos\theta}{\mu}$, X is the normalized distance given by x^*/l. The effect of channel geometry is realized via the factor $\beta h/3l$. The length taken by the membrane to relax back to zero deflection l_{rs} is assumed to be very small compared to the channel length l, which is verified through simulations (Table S1, supplementary material). The menisci start interacting only when the distance between them is smaller than the restoring length l_{rs}.

Next, we consider the case after the menisci cross each other and are sufficiently away from the crossing point (Figs. 1(e) and 1(f)). We consider that the pressure variation is linear along each liquid (i.e., increases from the meniscus toward upstream similar to Poiseuille flow) and thus realize an abrupt change in the pressure acting on the membrane p_m at each meniscus. This results in two deflection extrema at short distances after and before each meniscus. We can split the PC into five distinct regions (A to E) so the pressure acting on the membrane $p_m(x)$ (positive along the z-axis) is a split function (see Eq. (S3) in supplementary material). Deflection of membrane at any (x,y) is given by $\omega(x,y)=\delta(x)(1-4(\frac{y}{w})^2)^2$ except in regions B and D (high gradient), $\delta(x)$ is the maximum deflection at any x given by

$$\delta(x)=\alpha p_m(x)w^4/D, \quad \text{so } \xi=\frac{\delta}{h}=\frac{\alpha p_m(x)w^4}{Dh}. \tag{1}$$

Due to symmetry, $\delta(x)=-\delta(l-x)$. The deflection at the meniscus δ^* can be taken as an average of extrema $\delta^*=(\hat{\delta}+\delta')/2$ (verified using simulations, see Table S3 in supplementary material), where $\hat{\delta}$ and δ' are the extrema that

occur before and after the menisci, respectively. In the case of channels of high aspect ratios (i.e., $a \gg 1$), the Young-Laplace pressure drop across the meniscus located at x^* is given by

$$\Delta p_1 = 2\sigma\cos\theta\left(\frac{1}{h+\delta^*}+\frac{1}{w}\right) = \frac{2\sigma\cos\theta}{h}\left(\frac{1}{1+\xi^*}+\frac{1}{a}\right) \approx \frac{2\sigma\cos\theta}{h}\left(\frac{1}{1+\xi^*}\right) \approx \frac{2\sigma\cos\theta}{h}\left(\frac{1}{1+\frac{\hat{\xi}+\xi'}{2}}\right). \tag{2}$$

Also, using Eq. (S4) (supplementary material) and Eq. (1), we get

$$\Delta p_1 = -p_m(l-x') - p_m(\hat{x}) = \frac{Dh}{\alpha w^4}\left(\xi' - \hat{\xi}\right). \tag{3}$$

By eliminating Δp_1 from Eqs. (2) and (3) and accepting appropriate solution for ξ', we get $\xi' = -1+\sqrt{(1+\hat{\xi})^2+J}$. Using the modified cross-sectional area in Eq. (S5) (supplementary material) and flow rate in Eq. (S8) in supplementary material, the velocity of the meniscus in PC and the corresponding non-dimensional velocity, respectively, are obtained as

$$v = \frac{\beta D h^3 F_1(-\xi')}{12\mu\alpha\Gamma w^4(l-x^*)}, \quad \tilde{u} = \frac{1}{J}\left(\frac{\beta h}{3l}\right)\frac{F_1(-\xi')}{\Gamma(1-X)}. \tag{4}$$

Integrating the Eq. (S9) (supplementary material) in region C (i.e., from $x = (l-\hat{x})$ to $x = \hat{x} \approx x^*$ and $\xi = -\hat{\xi}$ to $\xi = \hat{\xi}$), we get the non-dimensional velocity of the meniscus as

$$\tilde{u} = \frac{1}{J}\left(\frac{\beta h}{3l}\right)\frac{F_2(\hat{\xi})}{\Gamma(2X-1)},$$
$$F_2(\xi) = \frac{683}{5000}\log\left(\frac{1.89-\xi}{1.89+\xi}\right) - \frac{3325}{5000}\tan^{-1}\left(\frac{8041}{6250}\xi\right). \tag{5}$$

The expression for ξ' along with Eqs. (4) and (5) is numerically solved using MATLAB to obtain the velocity of the meniscus at different positions after the crossing point.

Further, we consider the case at a very small instant after the crossing point where the menisci are still close to each other (Figs. 1(g) and 1(h)). The menisci cross each other at $x^* = l/2$ if the liquids are inserted into both channels at the same time. Following a similar approach as taken in the previous case, we realize that $p_m(x)$ is almost zero in the region between the menisci and $p_m(x)$ changes abruptly at each meniscus. Therefore, the membrane profile in the region between the menisci is monotonous without any deflection extrema ($\hat{\xi} = 0$). Maximum deflection ξ' occurs after the primary liquid meniscus x' and minimum deflection $(-\xi')$ occurs after the controlling liquid meniscus $(l-x')$. By solving Eq. (S11) (supplementary material) using $\xi^* = \xi'/2$ (simulations, valid with an error of 10%, supplementary material, Table S4), we obtain deflection of the membrane at crossing point $\xi'_c = -1+\sqrt{1+J}$. We can conclude that ξ'_c in the PC suddenly becomes positive (upward) at the crossing point (since J is positive). Thus, the pressure jump across the meniscus rapidly decreases leading to a sudden drop in the meniscus velocity at this point. Before the crossing point, the membrane deflection at the meniscus is negative (downward) ($\hat{\xi} = -1+\sqrt{1-J}$) (Eq. (S2), supplementary material). Similar to the case after the crossing point, the velocity of the meniscus at the crossing point is found by integrating the expression for R_1 from $x = 0$ to $x = (l-x')$ which results in $v_c = \frac{\beta D h^3 F_1(-\xi')}{12\alpha\mu\Gamma_c w^4(l-x')}$, the modified cross-sectional area $\Gamma_c = 1+\frac{4\xi'}{15}$ (Eq. (S12), supplementary material). The velocity of the liquid meniscus before the crossing point is given in Eq. (S13) (supplementary material). So the drop in the meniscus velocity is

$$\kappa = 1 - \frac{v_c}{v_s} = 1 - \frac{F_1(-\xi')\Gamma_c}{F_1(\hat{\xi})\Gamma_s}. \tag{6}$$

From Eq. (6), we observe that the percentage drop in the meniscus velocity is purely a function of J. Moreover, we can show that Eq. (6) remains the same even if liquids are inserted at different times. Therefore, the percentage drop in the velocity does not change with the location of the crossing point, which is verified using experiments.

Fig. 2 shows the variation of the meniscus velocity $\tilde{u} = (v/U_{cap})$ in the PC at different positions $X = x^*/l$ for different values of $J = 4\alpha\left(\frac{h}{l_{ec}}\right)^2 a^4$, which can be controlled by varying channel dimensions, membrane thickness, and liquid properties. At any location before the crossing point, meniscus velocity was found to be directly proportional to J. The PL meniscus velocity decreases from the inlet until the point where the menisci cross each other, i.e., $\tilde{x} = 0.5$; the rate of decrease was found to be independent of J. The

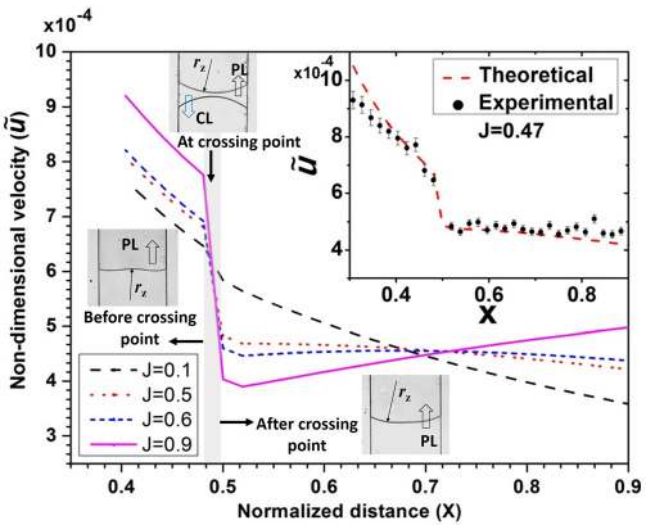

FIG. 2. Non-dimensional velocity of the PL meniscus $\tilde{u}$ with X predicted using the theoretical model, for different J values; (inset) Comparison of model predictions and experimental data (filled squares with error bars) for $\tilde{u}$ versus X for J = 0.47, error bars represent uncertainty in the experimental data due to the resolution of the scale; (inset) Experimental images showing PL and CL menisci shapes at different positions: before the crossing point, at the crossing point, and after the crossing point, the PL meniscus curvature is indicated by r_z, propan-1, 2-diol as working liquid and channel 1000 μm × 110 μm, fitting parameters: $l_{ec} = 1.352$ mm and $U_{cap} = 494.4$ mm/s.

decrease in velocity is attributed to the increase in viscous resistance as the capillary flow meniscus progresses. At the crossing point, a sudden drop in the meniscus velocity is observed for all J values due to the upward deflection of the membrane, as evident from $\xi_c' = -1 + \sqrt{1+J}$ in the model. Experiments were performed to study the variation of $\tilde{u}$ with X for different J values. Fig. 2 (inset) shows the comparison between model predictions and experimental data for $J = 0.47$, which shows a good agreement within 10%. Since PDMS is known to be gas permeable, the presence of nanoscale gas bubbles on the channel surface may also have influence on the capillary flow.[10,11] Although, consideration of this phenomenon is very challenging, this may be a source of error which is responsible for the deviation of the theoretical modeling results from the experimental data. The experimental data also show a sudden drop in velocity at the crossing point similar to the model. The change in the sign of ξ^* at the crossing point is also evident from the PL meniscus shape before and at the crossing point (insets in Fig. 2). Before the crossing point, the radius of curvature at the center of the meniscus r_z is negative indicating inward deflection of the membrane.[21,22] At the crossing point, r_z suddenly becomes positive, which is due to the outward deflection of the membrane.[5]

Model predictions show that the PL meniscus velocity decreases, remains constant, or increases after the crossing point depending on the value of J. At smaller J values i.e., $J < 0.5$, the membrane deflection toward the primary liquid is relatively smaller; thus, the change in height of the channel at the meniscus is insignificant. Consequently, the increment in the pressure drop across the meniscus Δp_m is lower as compared to that in the viscous pressure loss Δp_v so the meniscus velocity decreases downstream. After the crossing point, the downward pressure acting on the membrane decreases so consequently the height of the PC decreases which is evident from the increase in the radius of curvature of the meniscus r_z after the crossing point compared to that at the crossing point (inset in Fig. 2). For $J = 0.5$ to 0.6, the meniscus velocity remains almost constant downstream after the crossing point, which indicates a balance between the increment in the pressure jump across the meniscus Δp_m and that in the viscous pressure drop Δp_v. For $J > 0.6$, the meniscus velocity increases downstream since the increment in Δp_m is higher than that in Δp_v. Fig. 3 shows the variation of percentage drop in velocity (Eq. (6)) at the crossing point with J predicted using the model and obtained from experiments, which show good agreement within a maximum error of 15%. The percentage drop in velocity is found to increase with increase in the J value. As the J value increases, the change in the deflection at the crossing point ($\xi_c' - \hat{\xi}_s = \sqrt{1+J} - \sqrt{1-J}$) increases which leads to the increase in percentage drop in velocity. For $J = 1$, a maximum of 60% drop in the meniscus velocity is observed from both model and experiments just prior to the membrane collapse for $J > 1$. Experiments were performed by changing the time interval between the insertions of the liquids at the PC and CC inlets which showed that the percentage drop in the meniscus velocity at the crossing point is independent of the position of the crossing point (inset in Fig. 3).

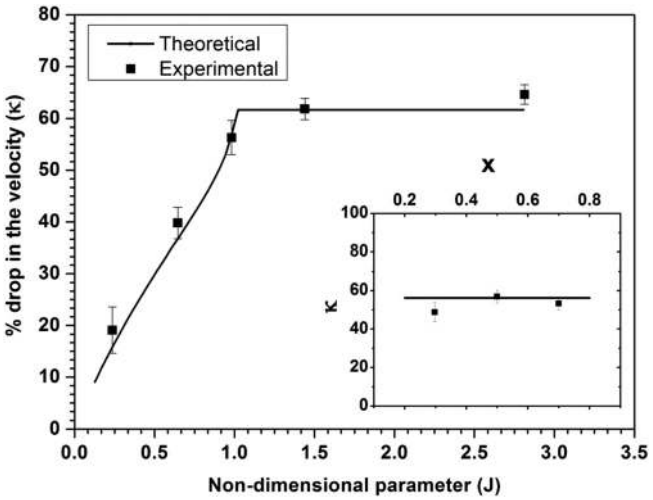

FIG. 3. Percentage drop in PL meniscus velocity $\tilde{u}$ with non-dimensional parameter J at the crossing point, theoretical predictions (solid line) and experimental data (filled squares with error bars), fitting parameter: $l_{ec} = 1.372$ mm, membrane collapses for $J > 1$ (inset) percentage drop in $\tilde{u}$ with positions of the crossing point X, channel 1000 μm × 75 μm, theoretical predictions (solid line) and experimental data (filled squares with error bars), error bars represent uncertainty in the experimental data due to the resolution of the scale.

In conclusion, we investigated the interaction of elasto-capillary flows in parallel microchannels across a thin membrane using theoretical model and experiments. At the crossing point, a significant drop (over 60%) in the meniscus velocity was observed for $J = 1$ prior to membrane collapse. After the crossing point, meniscus velocity decreases for $J < 0.5$, remains constant for $0.5 < J < 0.6$, and increases for $J > 0.6$. The proposed technique could be applied for passive control of capillary flows in microchannels. Also, it could motivate further research on the interaction between fluids and flows across thin membranes and compliant structures.

See supplementary material for the supporting derivations of the theoretical model and supporting data obtained using structural simulations.

The authors would like to thank the Department of Science & Technology, India (EMR/2014/001151), Department of Biotechnology, India (BT/PR7276/MED/32/267/2012), and I.I.T. Madras (MEE15-16843RFTPASHS) for providing the financial support. We also acknowledge CNNP, IIT Madras for supporting the photolithography work.

[1]D. Mark, S. Haeberle, G. Roth, F. von Stetten, and R. Zengerle, Chem. Soc. Rev. **39**, 1153 (2010).
[2]A. W. Martinez, S. T. Phillips, G. M. Whitesides, and E. Carrilho, Anal. Chem. **82**, 3 (2010).
[3]J. W. Van Honschoten, M. Escalante, N. R. Tas, H. V. Jansen, and M. Elwenspoek, J. Appl. Phys. **101**, 094310 (2007).
[4]R. Anoop and A. K. Sen, Phys. Rev. E. **92**, 013024 (2015).
[5]D. George, R. Anoop, and A. K. Sen, Appl. Phys. Lett. **107**, 261601 (2015).
[6]H.-Y. Kim and L. Mahadevan, J. Fluid Mech. **548**, 141 (2006).
[7]C. Duprat, J. M. Aristoff, and H. A. Stone, J. Fluid Mech. **679**, 641 (2011).
[8]D. M. Cate, J. A. Adkins, J. Mettakoonpitak, and C. S. Henry, Anal. Chem. **87**, 19 (2015).
[9]X. Li, D. R. Ballerini, and W. Shen, Biomicrofluidics **6**, 011301 (2012).
[10]F. Chauvet, S. Geoffroy, A. Hamoumi, M. Prat, and P. Joseph, Soft Matter **8**, 10738 (2012).

[11]V. N. Phan, N. T. Nguyen, C. Yang, P. Joseph, L. Djeghlaf, D. Bourrier, and A. M. Gue, Langmuir **26**, 13251 (2010).
[12]J. Atencia and D. J. Beebe, Nature **437**, 648 (2005).
[13]J. S. Rossier, G. Gokulrangan, H. H. Girault, S. Svojanovsky, and G. S. Wilson, Langmuir **16**, 8489 (2000).
[14]S. Lai, S. Wang, J. Luo, L. Lee, S. Yang, and M. Madou, Anal. Chem. **76**, 1832 (2004).
[15]R. Safavieh and D. Juncker, Lab Chip **13**, 4180 (2013).
[16]J. W. Suk and J.-H. Cho, J. Micromech. Microeng. **17**, N11 (2007).
[17]T. Vestad, D. W. M. Marr, and J. Oakey, J. Micromech. Microeng. **14**, 1503 (2004).
[18]P. Sajeesh, M. Doble, and A. K. Sen, Biomicrofluidics **8**, 054112 (2014).
[19]J. M. Aristoff, C. Duprat, and H. A. Stone, Int. J. Nonlinear. Mech. **46**, 648 (2011).
[20]K. A. Polzin and E. Y. Choueiri, J. Phys. D. Appl. Phys. **36**, 3156 (2003).
[21]J. W. van Honschoten, M. Escalante, N. R. Tas, and M. Elwenspoek, J. Colloid Interface Sci. **329**, 133 (2009).
[22]N. R. Tas, P. Mela, T. Kramer, J. W. Berenschot, and A. Van Den Berg, Nano Lett. **3**, 1537 (2003).